What happens structurally and chemically during sodium uptake and release by $Ni_2P_2S_6$: a combined X-ray diffraction, X-ray absorption, pair distribution and MAS NMR analysis

Jonas van Dinter[a], Kevin Synnatschke[b], Tobias A. Engesser[a], Sylvio Indris[c], Niklas Wolff[d], Ole Gronenberg[d], Martin Etter[e], Giannantonio Cibin[f], Lorenz Kienle[d], Claudia Backes[b] and Wolfgang Bensch*[a]

[a]*Institute of Inorganic Chemistry, University of Kiel, Max-Eyth-Str. 2, 24118 Kiel, Germany*

[b]*Institute for Physical Chemistry, Heidelberg University, Im Neunheimer Feld 253, 69120 Heidelberg, Germany*

[c]*Institute for Applied Materials - Energy Storage Systems, Karlsruhe Institute of Technology, P.O. Box 3640, 76021 Karlsruhe, Germany*

[d]*Institute for Materials Science, University of Kiel, Kaiserstr. 2, 24143 Kiel, Germany*

[e]*Deutsches Elektronen-Synchrotron (DESY), Notkestr. 85, Hamburg 22607, Germany*

[f]*Diamond Light Source, Harwell Science and Innovation Campus, Diamond House, Didcot, Oxfordshire OX11 0DE, United Kingdom*

Experimental

Liquid phase exfoliation and centrifugation

Ground crystals of $Ni_2P_2S_6$ (500 mg) were sonicated for 8 h in 80 mL of NMP using a sonic tip (Vibracell VCX, 750 W, horn tip, order number Z192732-1EA) at 60% amplitude in a 6 s on/4 s off pulse sequence. The dispersion was kept in a 4 °C cooling cell during sonication in order to avoid heating effects. The resulting dispersion was subjected to a 2-step centrifugation procedure (3000 *g* and 10000 *g*). After centrifugation at 3000 *g* in the first step, the supernatant was used for the subsequent step at 10000 *g*. The sediment obtained after the second centrifugation step was redispersed in reduced solvent volume (~1 mL NMP). The sample prepared according to this protocol is referred to as "exfoliated $Ni_2P_2S_6$". A Hettich Mikro 220R centrifuge equipped with a fixed-angle rotor (1195A) was used for both centrifugation steps for 2 h at 20 °C.

Atomic force microscopy

Atomic force microscopy (AFM) was carried out to determine lateral size and layer number of exfoliated $Ni_2P_2S_6$ on a Dimension ICON3 scanning probe microscope (Bruker AXS S.A.S.) in ScanAsyst in air under ambient conditions using aluminium coated silicon cantilevers (OLTESPA-R3). The concentrated dispersion was diluted with isopropanol to optical densities <0.1 at 500 nm. A drop of the dilute dispersion (15 µL) was deposited on pre-heated (180 °C) Si/SiO_2 wafers (0.5x0.5 cm^2) with an oxide layer of 300 nm. After deposition, the wafer was rinsed with ~10 mL of water and ~10 mL of isopropanol and dried with compressed nitrogen. Typical image sizes were 10x10 μm^2 at scan rates of 0.5 - 0.8 Hz with 1024 lines per image. Step-height analysis from previous work was used to convert the apparent AFM thickness to the layer number.[1] Previously published length corrections were used to correct lateral dimensions for cantilever broadening.[2]

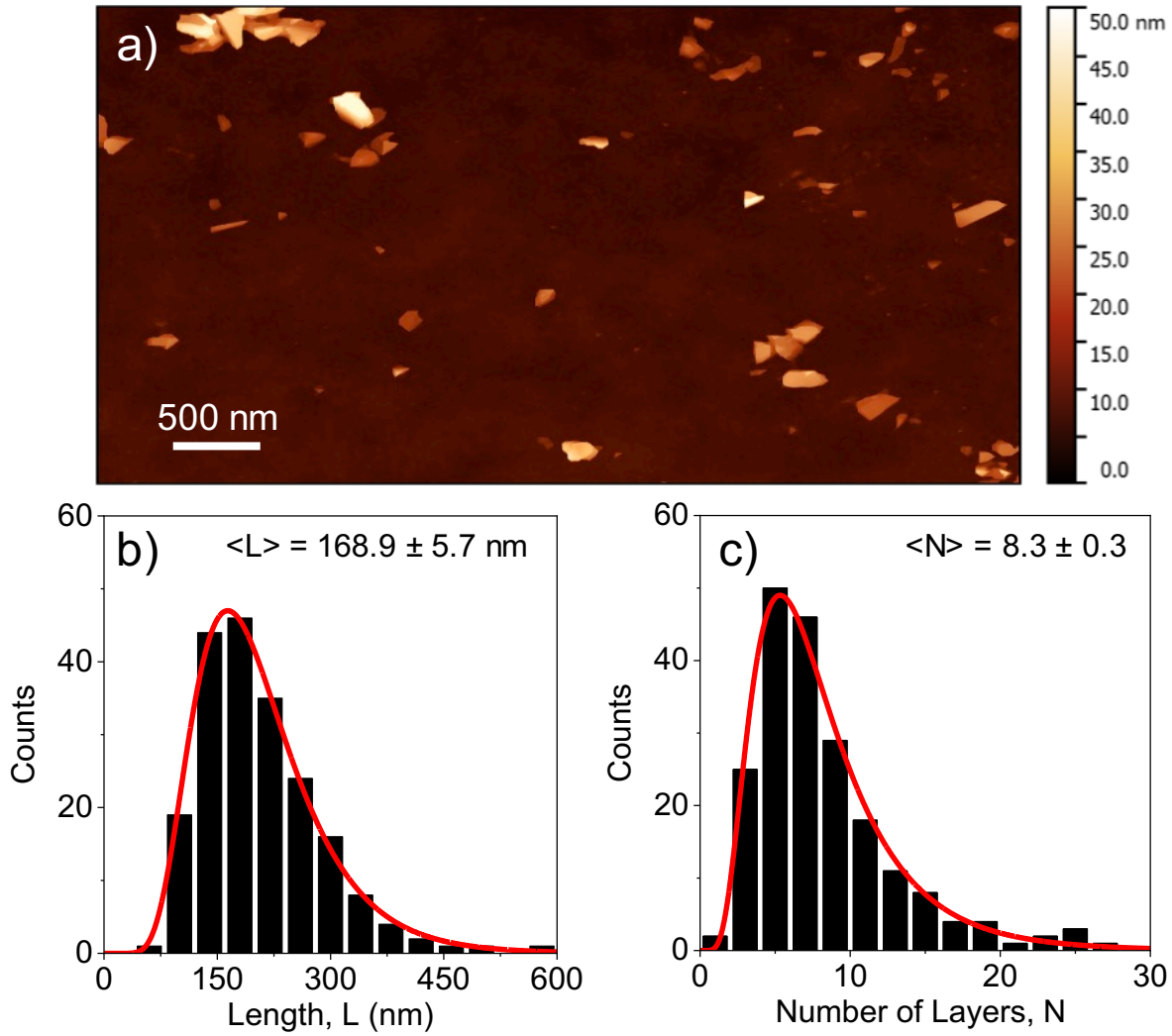

Figure S1. a) Representative AFM image of the exfoliated nanosheets. b, c) Histograms of lateral size, L and layer number, N of the exfoliated $Ni_2P_2S_6$ nanosheets. <L> and <N> are the arithmetic mean of the nanosheet lateral size and layer number.

Transmission electron microscopy

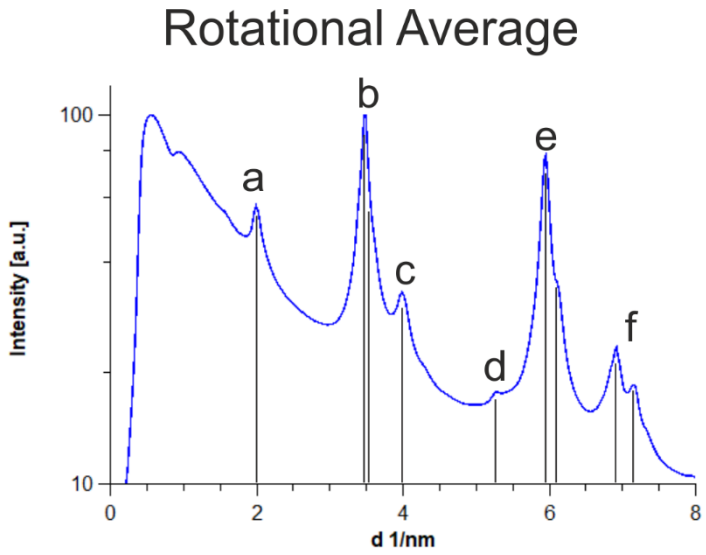

		a	b	c	d	e	f
d [Å]		5.02	2.86 || 2.80	2.51	1.89	1.68 || 1.62	1.44 || 1.40
C2/*m*	(hkl)	(020)	(130) || (200)	(040)	(150) / (240)	(060) || (330)	(260) || (170)
	d [Å]	5.041	2.876 || 2.781	2.520	1.896 / 1.867	1.680 || 1.623	1.438 || 1.394

Figure S2. Rotational intensity average of the diffraction pattern shown in Figure 2. The reflections can be indexed according to the monoclinic space group *C2/m*. The table displays the experimental lattice parameters d as well as a list of lattice parameters and lattice planes (hkl).

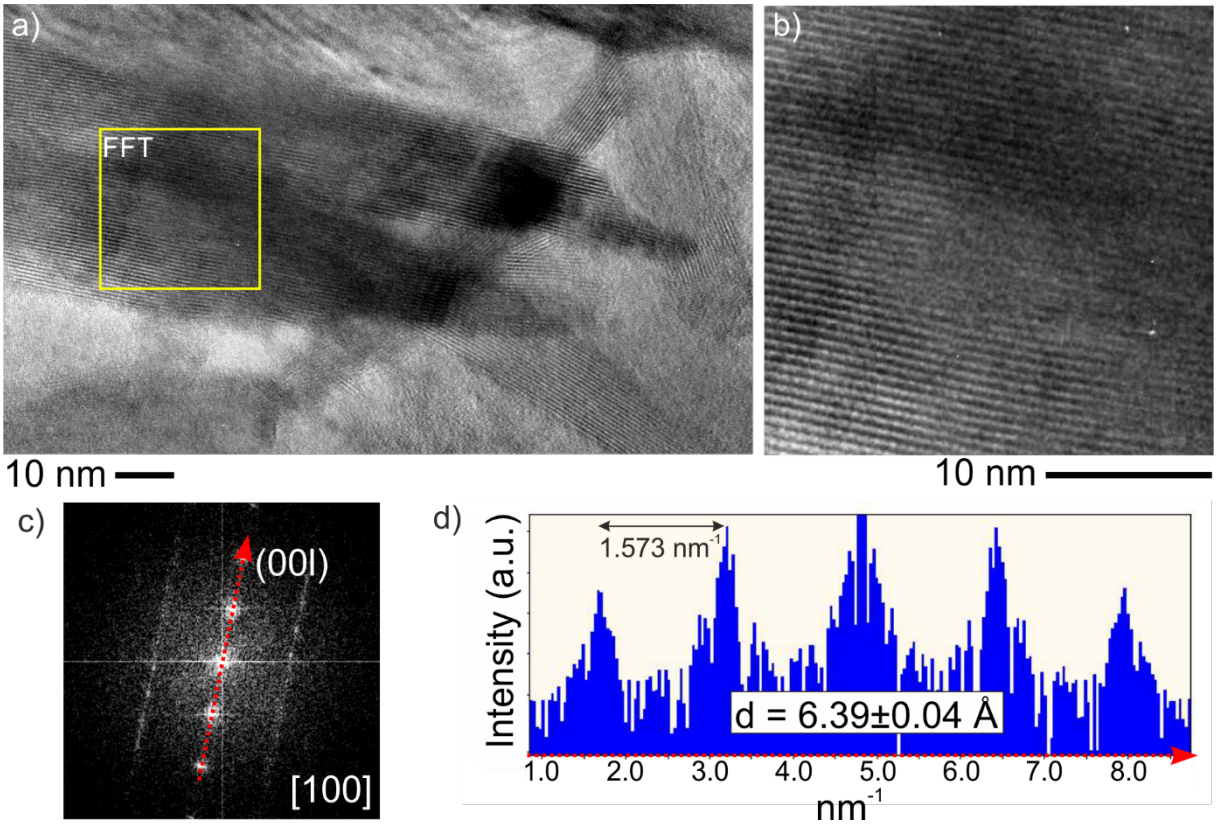

Figure S3. a, b) High-resolution TEM micrographs showing $Ni_2P_2S_6$ crystals coincidentally oriented along the [100] "edge-on" direction. c) In the FFT more or less pronounced diffuse streaking of the intensity in second order reflections is observed which indicates structural disorder between the crystal layers. d) The spacing between {00l} lattice planes was determined by evaluating the first order reflections appearing in the FFT.

Scanning electron microscopy and elemental analysis by EDX and CHNS

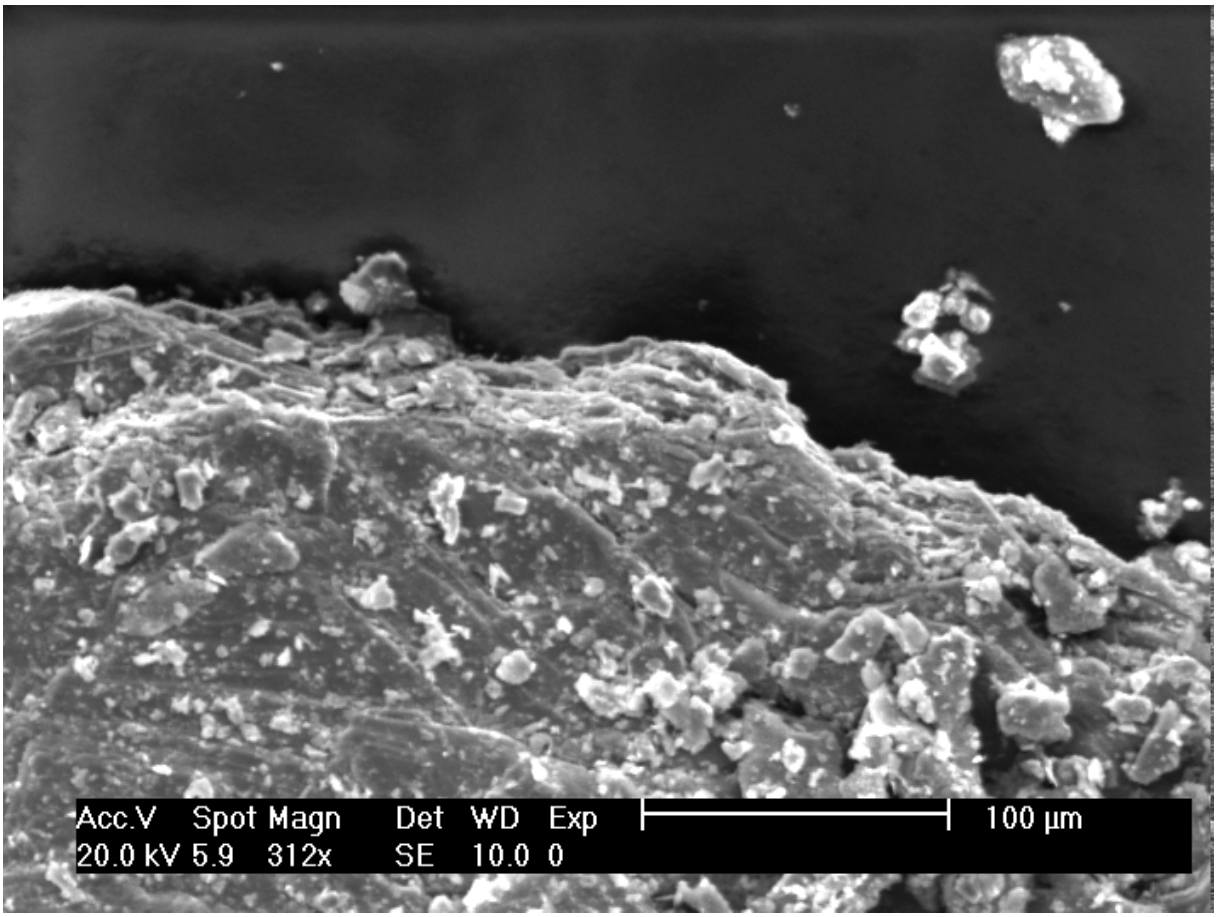

Figure S4. SEM images of $Ni_2P_2S_6$ sample showing its layered structure at the edges of the agglomerate.

Table S1. Results of EDX measurements of $Ni_2P_2S_6$ powder at different spots on the sample.

	Ni / at.%	P / at.%	S / at.%
Spot 1	22.56	21.50	55.94
Spot 2	22.28	20.88	56.84
Spot 3	23.55	20.96	55.49
Average	22.80 ± 0.56	21.11 ± 0.28	56.09 ± 0.56
Composition	$Ni_{2.28}P_{2.11}S_{5.61}$		

The SEM EDX measurements reveal stoichiometric ratios of Ni and P close to 1:1. The S content exhibits smaller values than expected from the target stoichiometry. This might be explained by the low energy of the S K_α emission line and absorption by the matrix. To account the S content properly, additional elemental (CHNS) analysis was conducted (Table S2).

Table S2. Results of the elemental analysis of the $Ni_2P_2S_6$ sample. As reference sulphanilamide was used. For the calculation of the composition, results of the elemental analysis were compared with the theoretical value of 51.76 wt.% S in $Ni_2P_2S_6$. This leads to compositions of $Ni_xP_xS_{6.10}$. Combining these results with the M:P ratio obtained from the EDX measurements, the total compositions of the samples were determined.

Sample	N / wt.%	C / wt.%	H / wt.%	S / wt.%
$Ni_2P_2S_6$	0.0	0.16	0.03	52.63
theoretical	0.0	0.0	0.0	51.76

Taking the results from the elemental analysis into consideration, the composition is calculated to be $Ni_{2.11}P_{1.81}S_{6.10}$.

Raman scattering

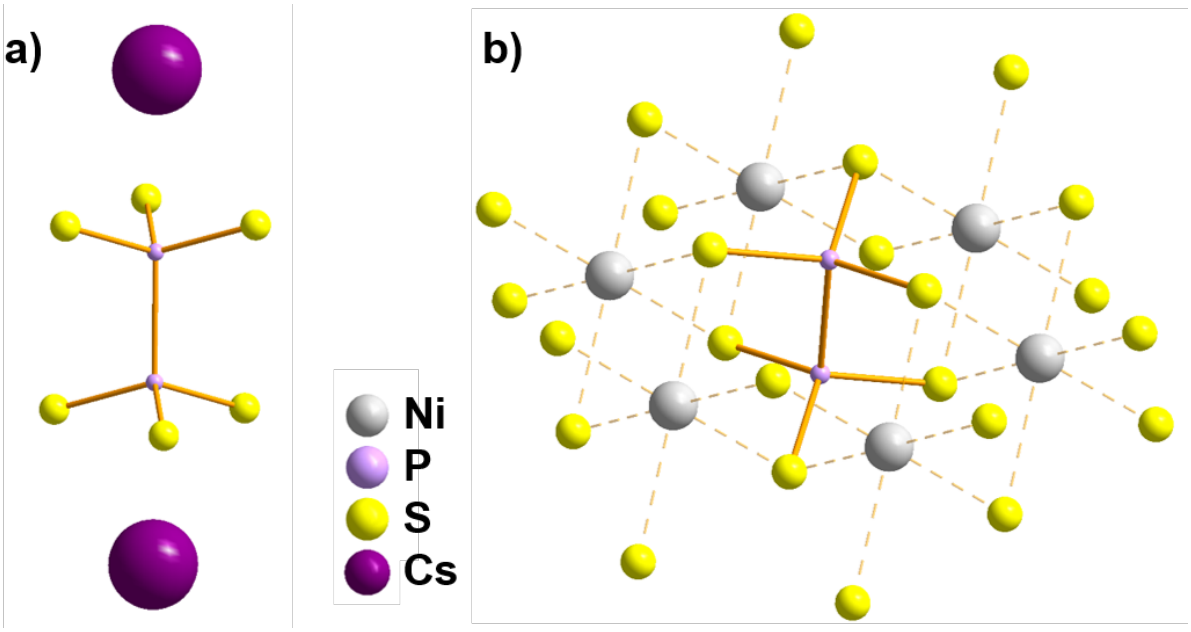

Figure S5. a) $[Cs_2(P_2S_6)]^{2-}$ anion with two Cs^+ cations on C_3 axis. b) $[Ni_6S_{18}(P_2S_6)]^{28-}$ fragment including $[P_2S_6]^{4-}$ anion and six nickel(II) ions as well as additional 18 sulfide anions (coordinates taken from the single crystal structure). Both structures show D_{3d} symmetry.

Table S3. Experimental and calculated frequencies of the Raman (Ra) and IR bands[a] of $Ni_2P_2S_6$ and model structures $[Ni_6S_{18}(P_2S_6)]^{28-}$ (D_{3d}) and $[Cs_2P_2S_6]^{2-}$ (D_{3d}) [cm^{-1}].

$Ni_2P_2S_6$ Exp.		$[Ni_6S_{18}(P_2S_6)]^{28-}$ Calc. PBE0/def2-TZVPP/ B3LYP/def2-TZVPP		$[Cs_2P_2S_6]^{2-}$ Calc. PBE0/def2-TZVPP/ PBE0/def2-QZVPP		Assignment	Activity
Raman	IR[b]	Raman	IR	Raman	IR	Mode Character χ	
-		-	-	-	33	A_{1u}	inactive
133		-	-	-	-	-	-
-		-	130/129	-	135	E_u	IR
-		-	213/217	-	-	A_{1u}	inactive
177		229/219	-	159	-	$E_g^{(1)}$	Ra
255		215/216	-	186	-	$A_{1g}^{(1)}$	Ra
-		-	229/234	-	213	E_u	IR
282		251/253	-	240	-	$E_g^{(2)}$	Ra
-		-	268/264	-	306	A_{2u}	IR
385		411/406	-	373	-	$A_{1g}^{(2)}$	Ra
-	446	-	478/474	-	441	A_{2u}	IR
561	-	618/610	-	555	-	$E_g^{(3)}$	Ra
-	573	-	621/611	-	562	E_u	IR
589	-	608/600	-	532	-	$A_{1g}^{(3)}$	Ra
728-833	-	-	-	-	-	-	overtones/ unclear
1156-1202	-	-	-	-	-	-	overtones/ unclear

[a] Bands which correspond to Cs- or Ni-S- vibrations are assigned as lattice vibrations and not included. [b] IR spectrum was measured between 4000-400 cm^{-1}.

Electrochemical measurements: cyclic voltammetry

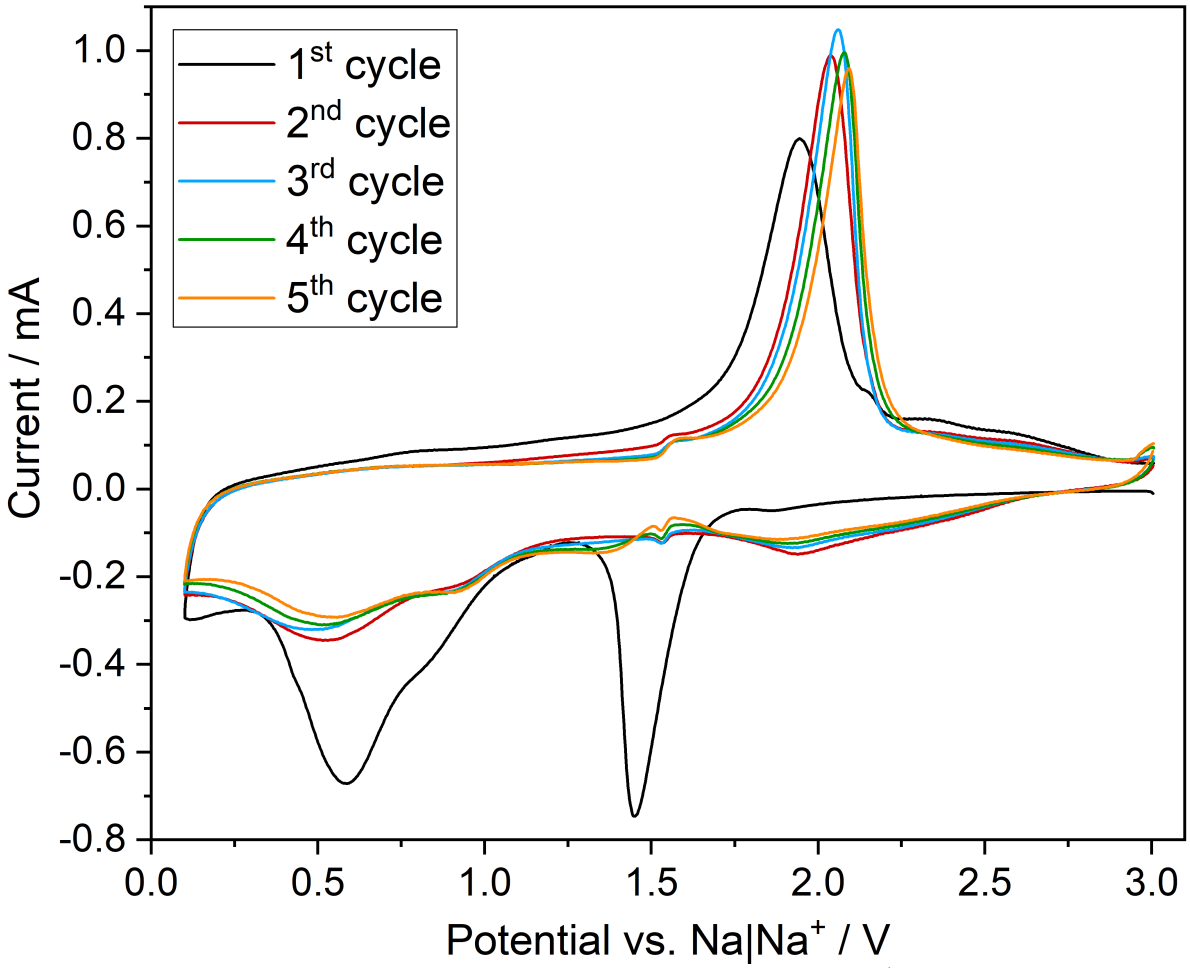

Figure S6. Cyclic voltammetry curves recorded with a scan rate of 0.1 mV s^{-1} in a potential window from 3.0 to 0.1 V.

For further electrochemical characterization, CV curves of the active material were recorded in a potential range from 3.0 V to 0.1 V. The pronounced difference between the first and the following cycles is characteristic for conversion-type reaction mechanisms. During the first discharge, a sharp reduction peak at 1.45 V and several not well-resolved peaks between 0.82 V and 0.43 V are observed. The sharp peak at 1.45 V is assigned to the reduction of Ni^{2+} to Ni, which is in good agreement with conducted *ex situ* measurements as well as with the discharge profile of the 1st cycle (see Fig. 4B). *Ex situ* measurements proof the complete reduction of Ni^{2+} between the uptake of 3.5 to 5 Na/f.u. The discharge profile of the 1st cycle exhibits an electrochemical plateau beginning at 1.45 V, which ends after a specific capacity of ~270 mAh g^{-1} was reached, corresponding to the uptake of roughly 4 Na/f.u. The reduction peaks between 0.82 V and 0.43 V are assigned to the presence of intermediate P and Na containing phases between the uptake of 5 to 9 Na/f.u. as well

as to the formation of Na_2S, which is in good agreement with the *ex situ* ^{23}Na and ^{31}P MAS NMR measurements. During charging, only one sharp oxidation peak occurs at 1.95 V with a very small shoulder at 2.14 V, which might be assigned to desodiation and oxidation of metallic Ni. In the second cycle, the sharp reduction peak slightly shifted to 1.53 V while losing nearly all of its initial intensity. The other reduction events occur at 0.91 V and 0.51 V. The oxidation peak is observed at 2.04 V in the second cycle with increased intensity.

The CV curves clearly demonstrate battery-type rather than pseudocapacitive behavior which is why pseudocapacity was not calculated, as it is not applicable for this type of energy device.[3–5]

Electrochemical long-term cycling of nanosheet $Ni_2P_2S_6$

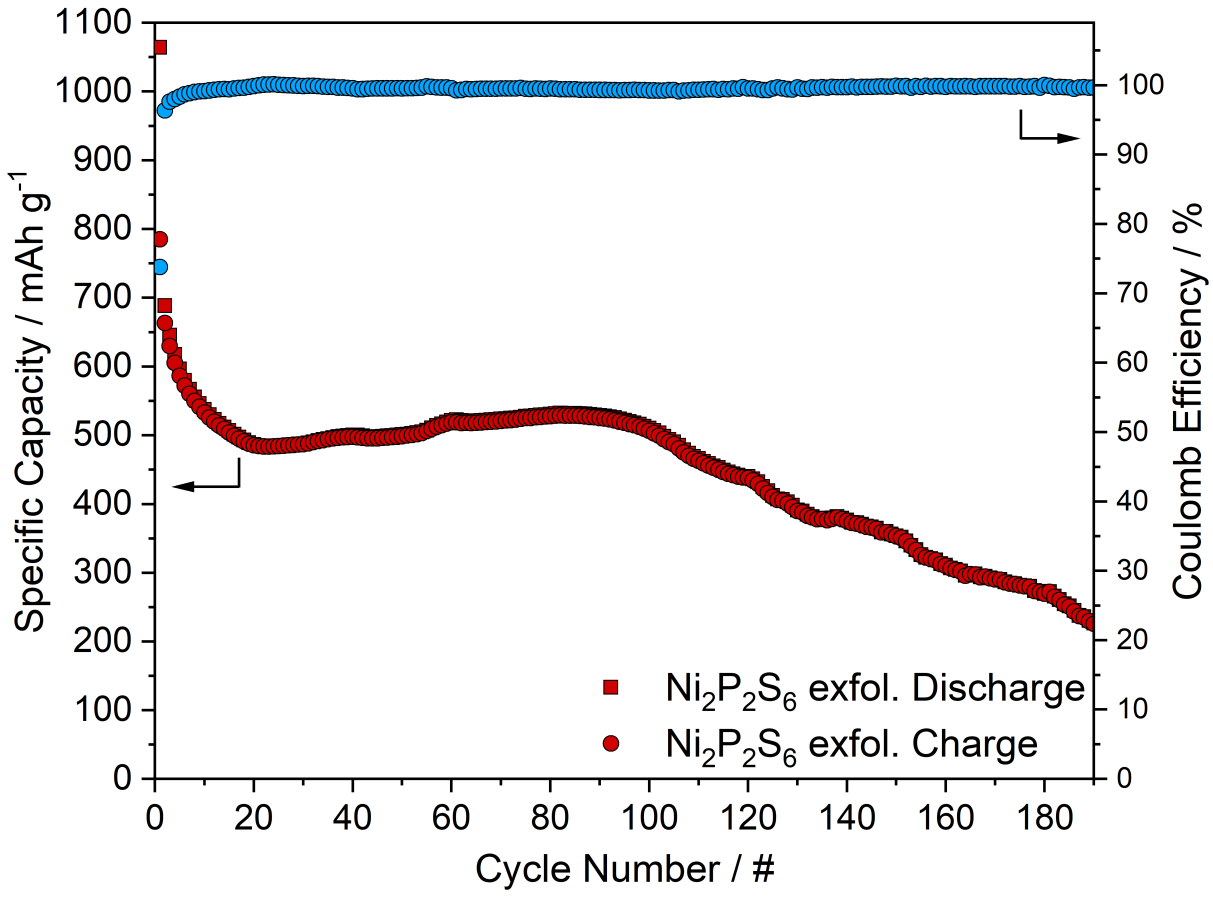

Figure S7. Electrochemical performance of nanosheet samples of $Ni_2P_2S_6$ against Na. Current rates of 1 A g^{-1} were applied within a potential window of 3.0 – 0.1 V.

Ex situ methods: X-ray diffraction, ^{19}F MAS NMR, pair distribution function analysis and X-ray absorption spectroscopy

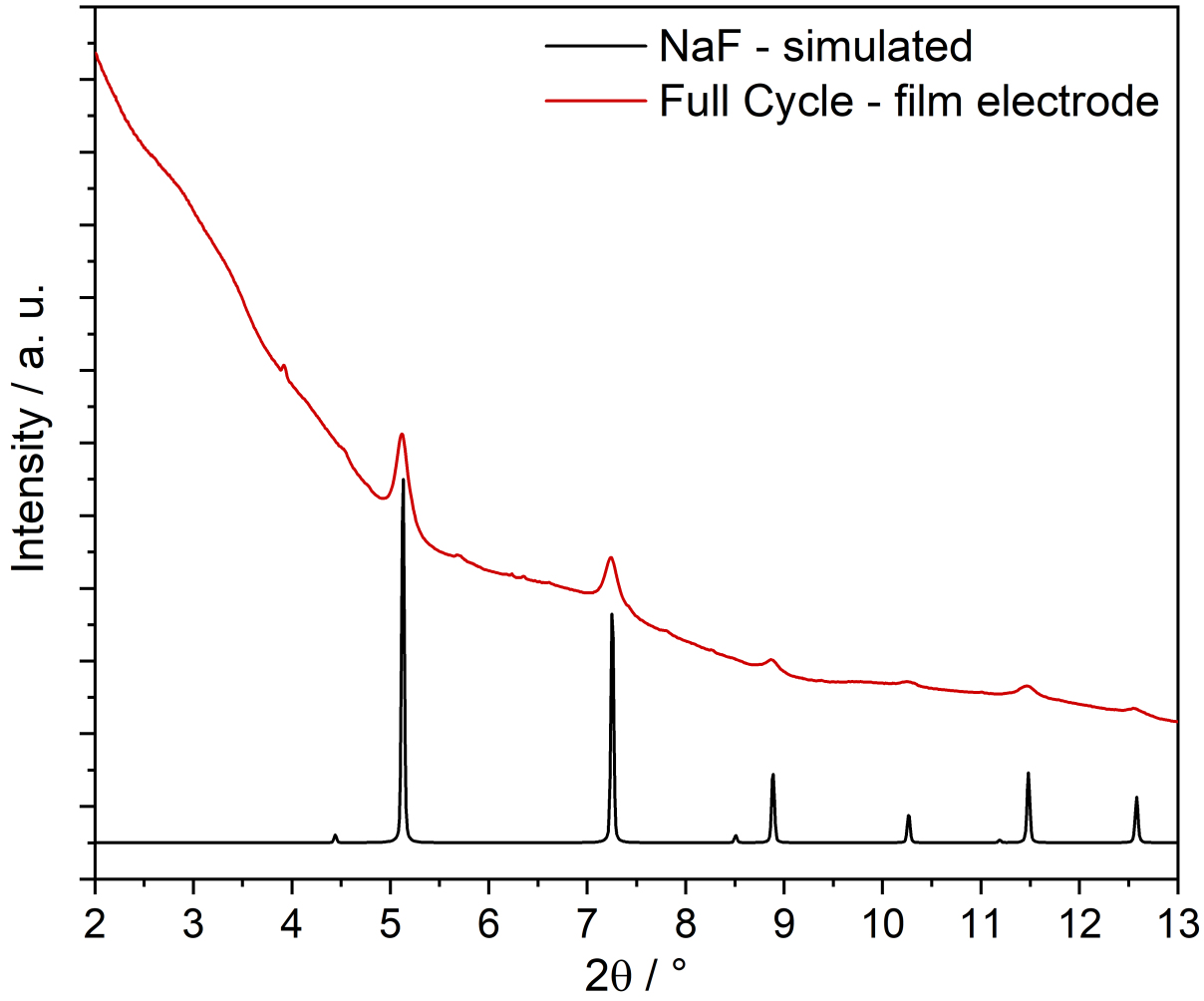

Figure S8. *Ex situ* X-ray diffraction pattern of the $Ni_2P_2S_6$ electrode collected after a full cycle compared to the calculated X-ray diffraction pattern of NaF.[6] Measured at beamline P02.1, DESY using 60 keV (λ = 0.207 Å).

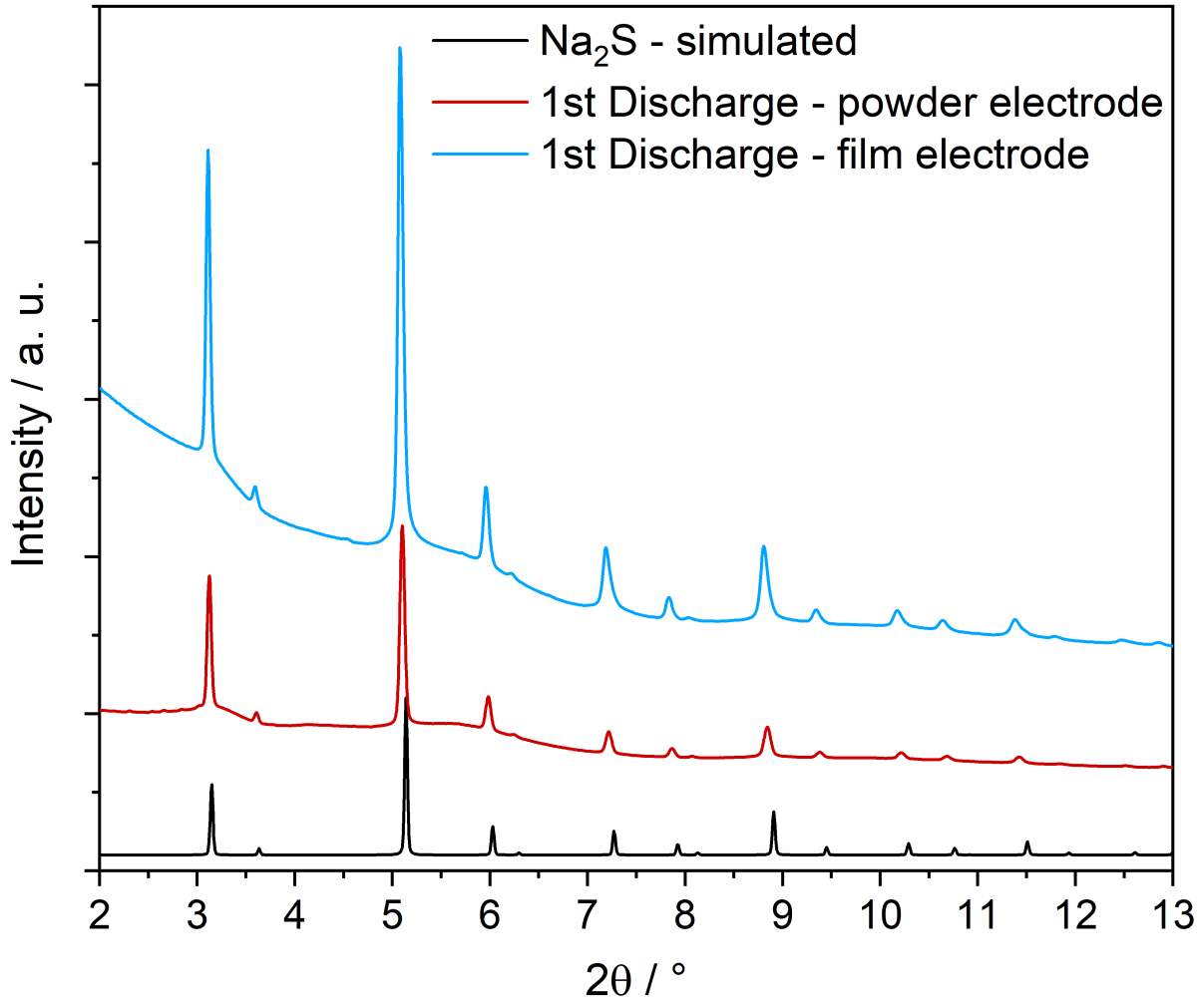

Figure S9. *Ex situ* X-ray diffraction pattern of $Ni_2P_2S_6$ film and powder electrodes collected after complete discharge compared to the calculated X-ray diffraction pattern of Na_2S.[7] The slight variations in peak position are most likely due to the nanoscale and disorder of the particles formed during the electrochemical reaction. The formation of Na_2S is evident in both cases, but no reflections of NaF are observed. Measured at beamline P02.1, DESY using 60 keV (λ = 0.207 Å).

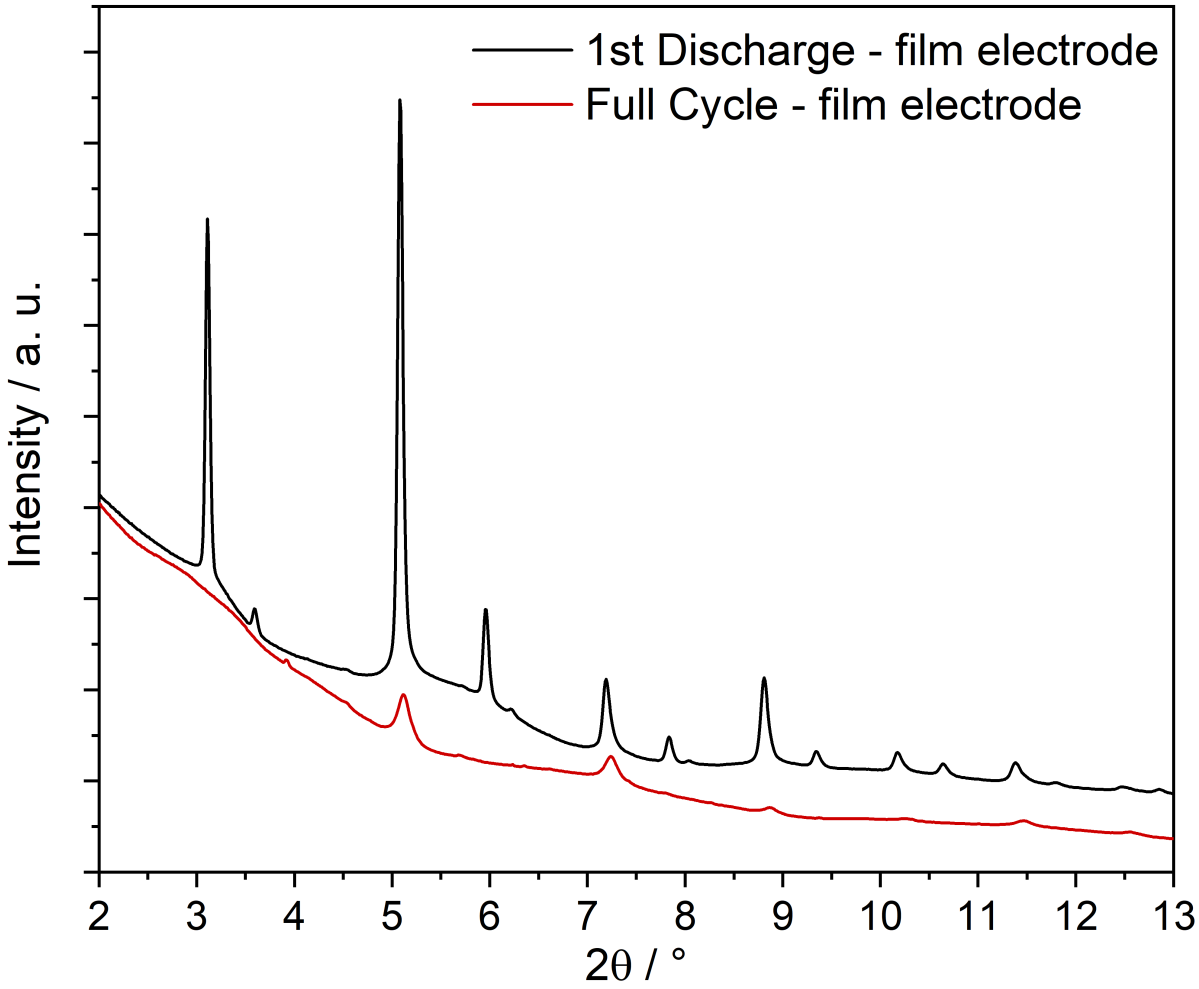

Figure S10. *Ex situ* X-ray diffraction pattern of the $Ni_2P_2S_6$ electrode on copper foil collected after a complete discharge and after a full cycle. In the completely discharged sample, reflections of Na_2S could possibly superpose the less intense reflections of NaF. Measured at beamline P02.1, DESY using 60 keV (λ = 0.207 Å).

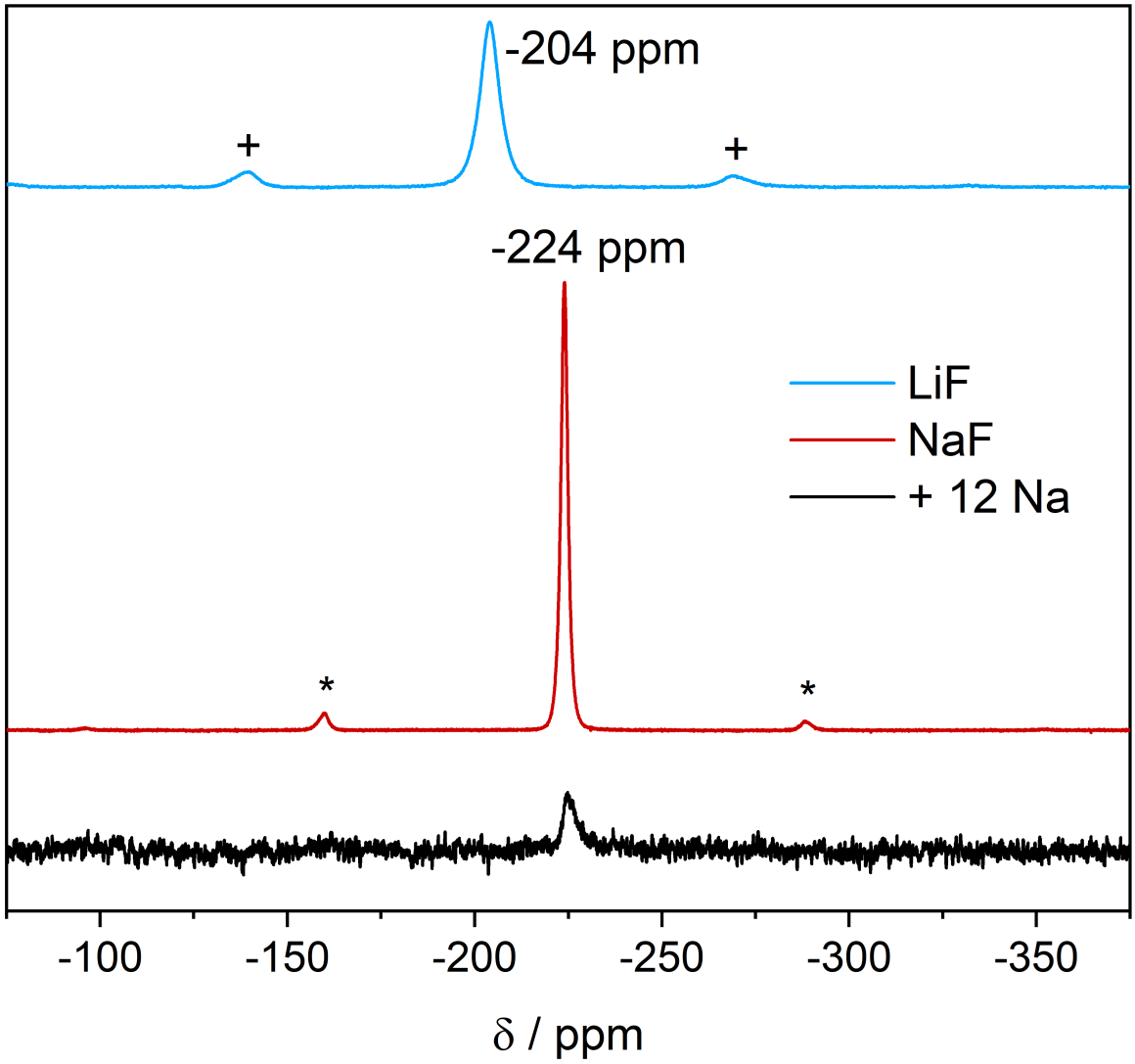

Figure S11. ^{19}F MAS NMR spectra of $Ni_2P_2S_6$ powder electrodes after a complete discharge compared to the references of NaF and LiF. Peaks marked with * and + visualize the spinning sidebands of the reference samples. The spectrum of the discharged sample was magnified by a factor of 200.

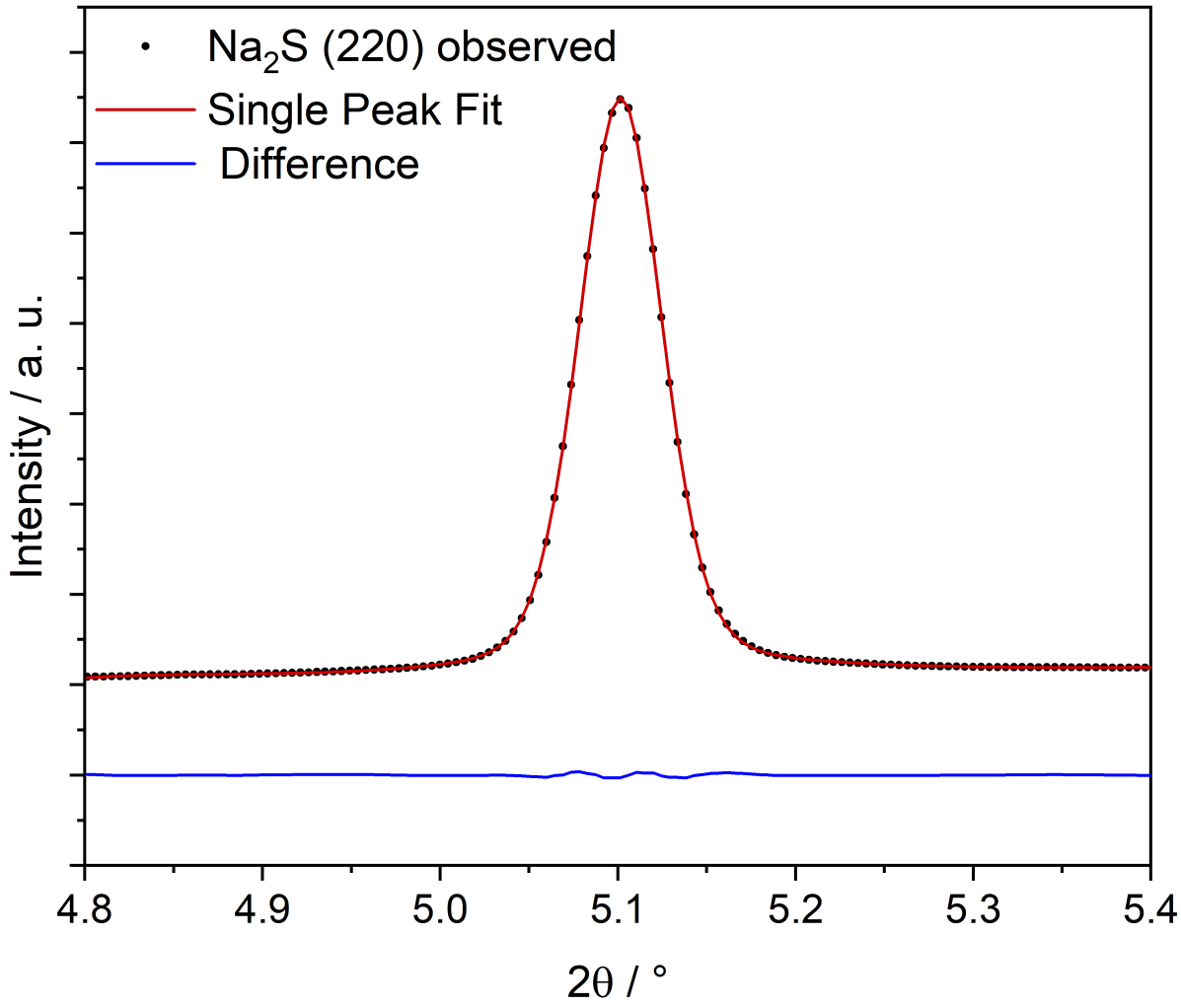

Figure S12. Single peak fit of the *ex situ* X-ray diffraction pattern of the completely discharged $Ni_2P_2S_6$ electrode. The (220) reflection of Na_2S is shown (black) with a single peak fit with a FWHM modelled by the Scherrer formula (red) and difference calculation (blue). Measured at beamline P02.1, DESY using 60 keV (λ = 0.207 Å).

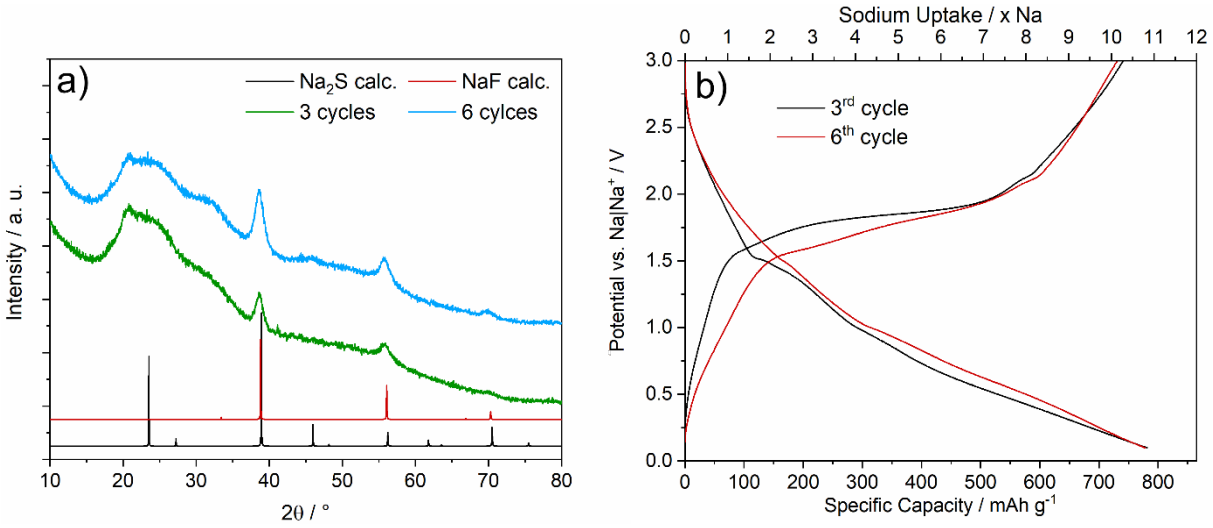

Figure S13. a) *Ex situ* X-ray diffraction pattern (Cu-Kα radiation (λ = 1.54058 Å) of the $Ni_2P_2S_6$ electrode on copper foil collected after 3 and 6 cycles (charged) compared to the calculated X-ray diffraction patterns of NaF[6] and Na_2S.[7] b) Discharge and charge profiles of the 3rd and 6th cycle of $Ni_2P_2S_6$ electrode. C-rates of C/10 and C/5 were applied for the sample cycled for 3 and for 6 cycles, respectively.

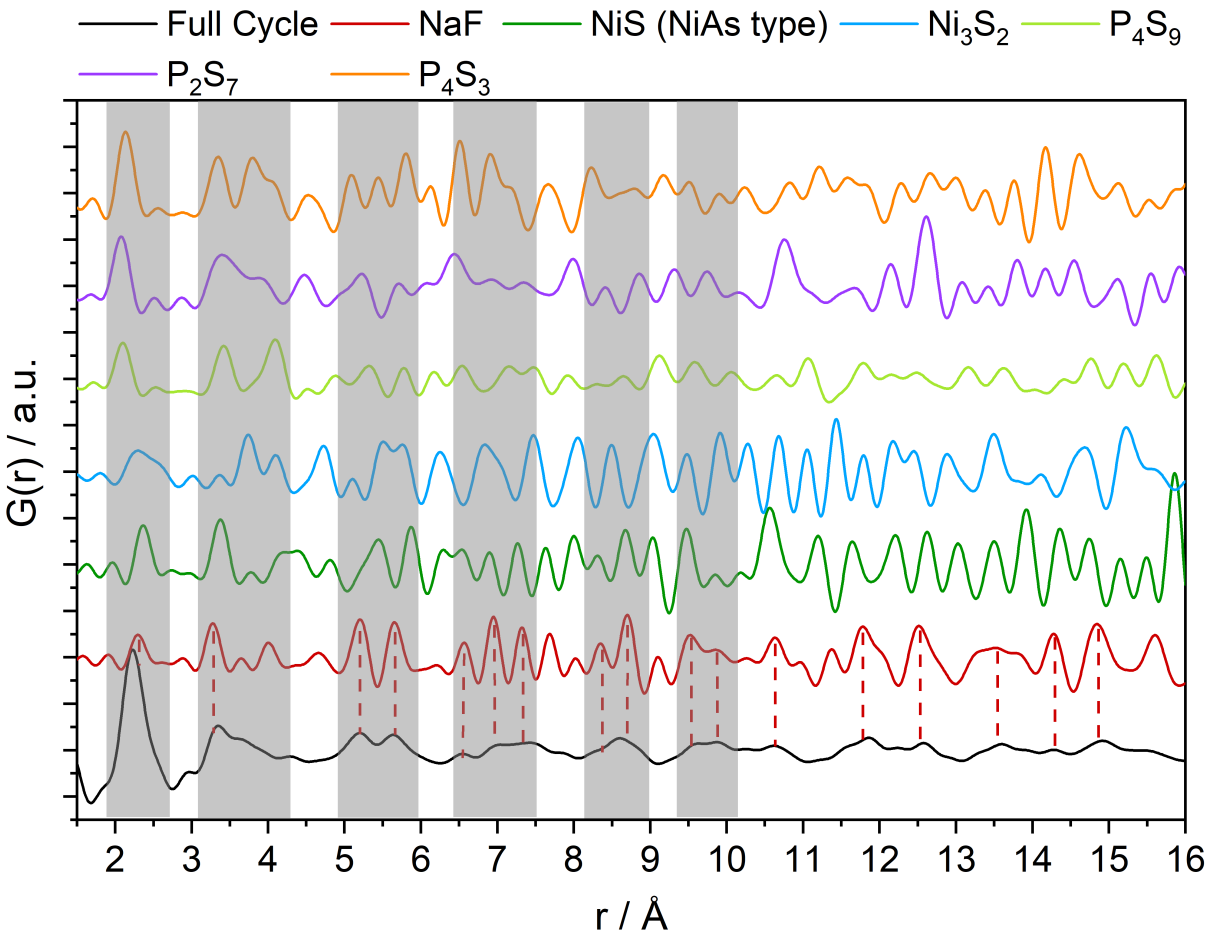

Figure S14. *Ex situ* pair distribution function of the $Ni_2P_2S_6$ electrode collected after a full cycle compared to the calculated PDF of NaF[6], NiS (NiAs type)[8], Ni_3S_2[9] , P_4S_9[10], P_2S_7[11] and P_4S_3[12]. The grey markings show areas where the different compounds have similar distances and therefore could

contribute to the PDF of the sample. The red dashed lines point out distances of NaF, which are in accordance with the PDF of the fully recharged sample.

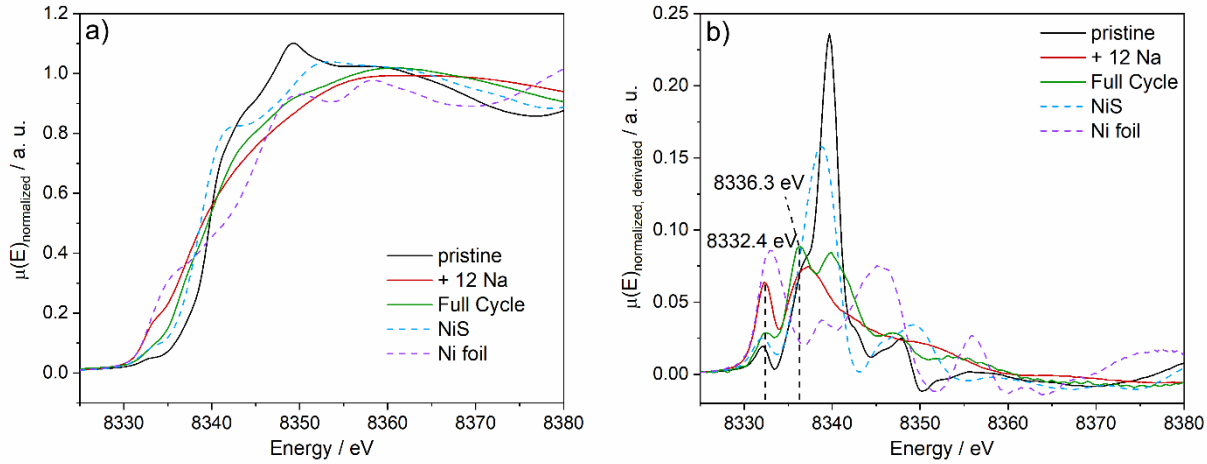

Figure S15. a) *Ex situ* XANES spectra at the Ni K-edge of the $Ni_2P_2S_6$ electrode after a full cycle compared with pristine and completely discharged $Ni_2P_2S_6$ as well as Ni foil and NiS and b) the corresponding first derivatives.

References

1 K. Synnatschke, S. Shao, J. van Dinter, Y. J. Hofstetter, D. J. Kelly, S. Grieger, S. J. Haigh, Y. Vaynzof, W. Bensch and C. Backes, *Chem. Mater.*, 2019, **31**, 9127–9139.

2 L. Ueberricke, J. N. Coleman and C. Backes, *Phys. Status Solidi B*, 2017, **254**, 1700443.

3 P. Simon, Y. Gogotsi and B. Dunn, *Science*, 2014, **343**, 1210–1211.

4 T. Brousse, D. Bélanger and J. W. Long, *J. Electrochem. Soc.*, 2015, **162**, A5185–A5189.

5 C. Costentin and J.-M. Savéant, *Chem. Sci.*, 2019, **10**, 5656–5666.

6 Y. Shirako, Y. G. Shi, A. Aimi, D. Mori, H. Kojitani, K. Yamaura, Y. Inaguma and M. Akaogi, *J. Solid State Chem.*, 2012, **191**, 167–174.

7 E. Zintl, A. Harder and B. Dauth, *Z. Elektrochem. Angew. Phys. Chem.*, 1934, **40**, 588–593.

8 N. Alsén, *Geol. Fören. Förh.*, 1925, **47**, 19–72.

9 M. E. Fleet, *Am. Mineral.*, 1977, **62**, 341–345.

10 W. Hilmer, *Acta Crystallogr., Sect. B: Struct. Sci., Cryst. Eng Mater.*, 1969, **25**, 1229–1232.

11 T. Rödl, R. Weihrich, J. Wack, J. Senker and A. Pfitzner, *Angew. Chem. Int. Ed.*, 2011, **50**, 10996–11000.

12 I. Raabe, S. Antonijevic and I. Krossing, *Chem. – Eur. J.*, 2007, **13**, 7510–7522.